Sensor and Simulation Notes

Note 337

Prepulse Associated with the TEM Feed of an Impulse Radiating Antenna

Everett G. Farr
Farr Research

Carl E. Baum
Phillips Laboratory

March 1992

Abstract

The field radiated from an impulse radiating antenna (IRA) utilizing a reflector and driver by a step-function source consists of three distinct parts. First, there is a prepulse, which looks ike a step function, and lasts for a time equal to twice the electrical length of the feed. Following this comes the actual impulse-like waveform. Finally, there is a small tail that appears after the impulse. Although the impulse portion of the waveform has been analyzed elsewhere, the prepulse has been only approximated. The purpose of this note is to provide simple analytical formulas for calculating the prepul.e for the two most common feed types, two bent circular cones, and two conical coplanar plates.

By generating simple formulas for the forward and backward radiation on axis, one can compare the area of the prepulse to that of the impulse. After doing so, it is easy to identify cases where the areas of the impulse and prepulse are equal, to within a very small tolerance. Since the total area under the waveform must be zero, this suggests that the tail after the impulse has zero area, a necessary condition for making the tail small.

I. Introduction

The field radiated from the impulse radiating antenna utilizing a reflector consists of three distinct parts. The first of these is the direct radiation from the feed structure, which is of rather low magnitude, but lasts for a fairly long time. This is followed by an impulse, which lasts for a brief time and is high in amplitude. Finally, there is a tail expected after the impulse. It is tempting to concentrate one's analysis of the IRA on the impulse, since radiating an impulse is the purpose of an IRA. However, it is also of considerable interest to understand exactly the nature of the prepulse, since the areas under the prepulse and impulse are comparable in magnitude. If the areas are equal, then one would expect a relatively small tail after the impulse, which would be a desirable characteristic for a broadband radiator. The purpose of this paper is to present simple closed-form expressions for the magnitude of the prepulse. This is done for two common feed configurations, two bent circular cones and two coplanar conical plates. Once the prepulse of the waveform is expressed simply, it is then easy to compare the area under the prepulse to that under the impulse. The final result is that it is simple to find cases where, to a very good approximation, the two areas are equal. This indicates that with proper tuning of the matching circuit, it should be possible to tune away most, if not all, of the tail.

The utility of the impulse radiating antenna (IRA) has been demonstrated in a number of papers. It was first observed in [1] that one could feed a paraboloidal reflector with a TEM feed which could be made to give balanced electric and magnetic dipoles at low frequency. Such an arrangement provides a compromise between high-frequency and low-frequency characteristics for radiating impulses, and is closely related to the concept of the Balanced Transmission-line Wave sensor. The Balanced Transmission-line Wave (BTW) sensor had recently been developed as a $\vec{p} \times \vec{m}$ sensor, whose low-frequency properties were such that they provided a $1 + \cos(\theta)$ pattern [2]. The receiving characteristics of such a $\vec{p} \times \vec{m}$ antenna were examined in [15]. A variety of methods of feeding the IRA have been suggested [3]. A calculation of the aperture efficiency of the IRA has been made, which showed that the aperture efficiency could be expressed in a simple closed form [4]. Finally, a numerical calculation was made, which approximated the entire radiated waveform on boresight [5].

A diagram of a typical IRA is shown in Figure 1. It consists of a conical transmission line structure feeding into and attaching to a parabolic reflector. Suitable loads are placed between the transmission-line feed and the dish in order to reduce reflections and provide the matched load required of the BTW. At the apex of the feed, a step-function voltage drives the antenna. An idealized radiated field is shown in Figure 2. It consists of a prepulse caused by direct radiation of the currents on the feed, followed by the impulse formed by the reflector, followed by a still-unknown tail. Since the total area under the waveform must be zero, if the area under the prepulse is equal to the area under the impulse, then it should be possible to make the tail waveform small.

In order to calculate the prepulse radiation, it is first necessary to provide a stereographic transformation to project a spherical geometry onto a planar surface. Since the standard

2

transformation has a singularity at exactly the position we are interested in, we have to establish a so-called reverse stereographic projection to handle this case. Once this is done, spherical geometries are easily transformed into cylindrical ones, and the resulting cylindrical geometries are solved using conformal mapping. This is done for both the bent circular cones and the coplanar conical plates. It is shown that the fields on boresight for both cases are similar. Finally, for the case of two bent circular cones, the area under the prepulse is compared to the area under the impulse.
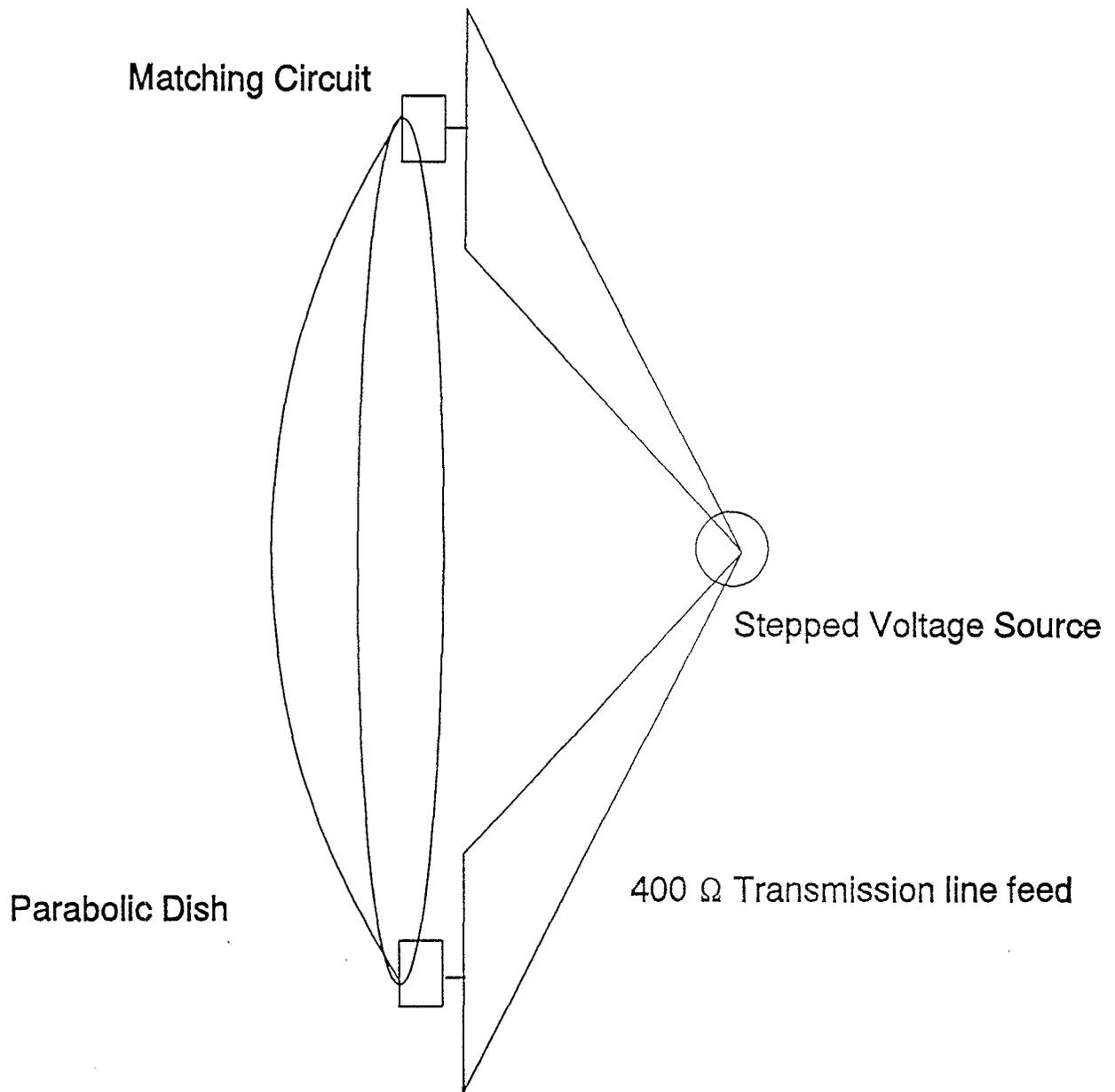
Figure 1. An impulse radiating antenna.
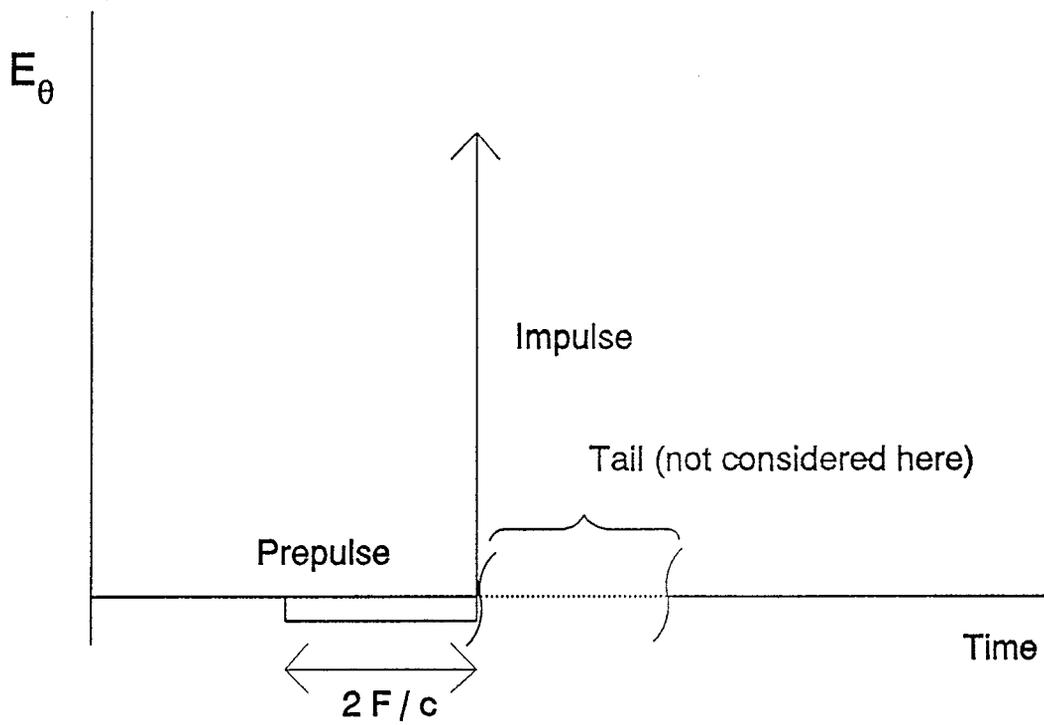
Figure 2. Idealized IRA waveform.

II. The Forward and Reverse Stereographic Projections

The theory needed to transform a spherical TEM wave into a cylindrical one is well established. In this section that theory will be reviewed, and a method will be introduced that handles the singularity for field radiated in the backward direction.

The geometry to be analyzed is shown in Figure 3. It consists of two circular cones of half-angle α at angles of β above and below the plane of symmetry. The procedure for analyzing the TEM waves that propagate on this structure is well known. Briefly, the potential on such a structure, at a constant radius satisfies a two dimensional Laplace's equation in spherical coordinates of the form

$$\sin\theta \frac{\partial}{\partial\theta}\left[\sin\theta \frac{\partial}{\partial\theta} V(\theta,\phi)\right] + \frac{\partial^2}{\partial\phi^2} V(\theta,\phi) = 0 \tag{1}$$

When one makes the substitutions

$$\theta = 2\arctan\left[\frac{(x^2+y^2)^{1/2}}{2r}\right] \tag{2}$$

$$\phi = \arctan(y/x)$$

which is the inverse of

$$x = 2r\tan(\theta/2)\cos(\phi) \tag{3}$$
$$y = 2r\tan(\theta/2)\sin(\phi)$$

one gets the simpler expression

$$\frac{\partial^2}{\partial x^2} V(x,y) + \frac{\partial^2}{\partial y^2} V(x,y) = 0 \tag{4}$$

This, of course, is just a two-dimensional Laplace's equation in cylindrical coordinates. This technique is equivalent to projecting a sphere of constant radius onto a plane. A diagram is shown in Figures 4 and 5. Figure 4 shows a three dimensional view of the projection, and Figure 5 shows a two-dimensional view in the y-z plane. Figure 4 is from [9].

This method has been described previously in [6], and has been implemented in a number similar applications [7-10]. It does, however, have a small difficulty when one wants to know the fields at $\theta=\pi$. At that angle, $\tan(\theta/2)$ approaches infinity, so one cannot use the transformation (3) simply.

6
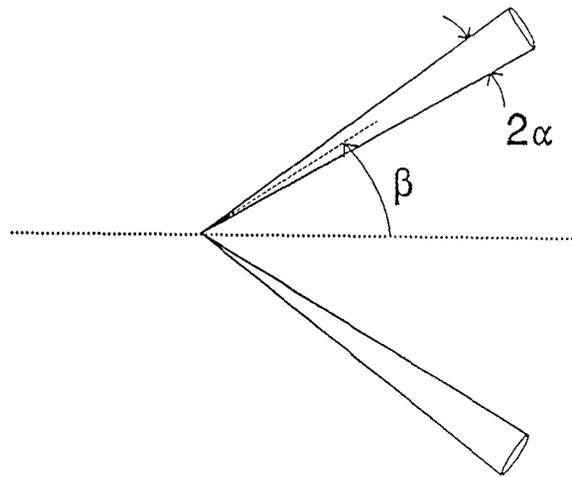
Figure 3. The bent circular cone structure to be analyzed.
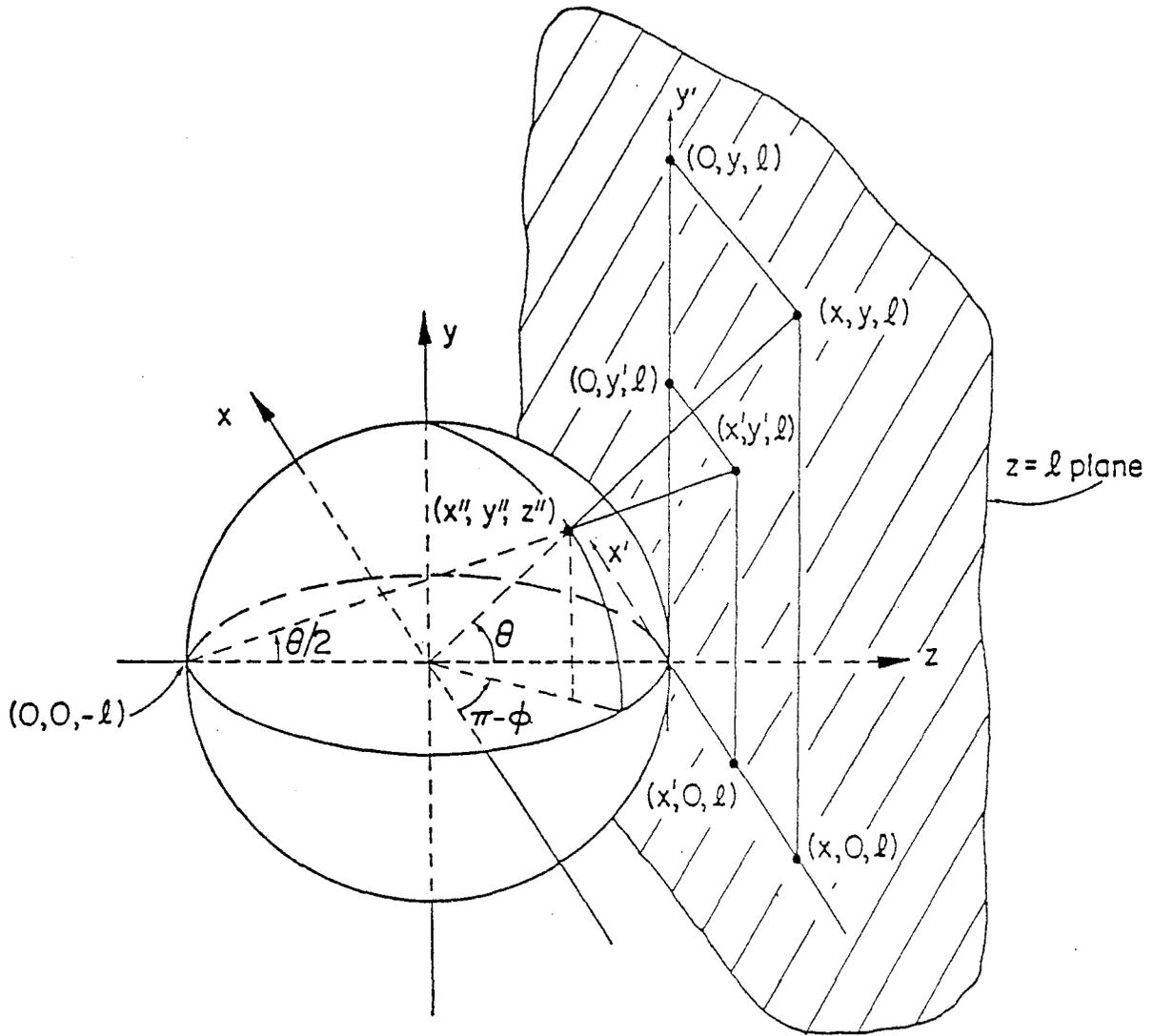
Figure 4. A 3-dimensional view of the stereographic projection, from [9].

8
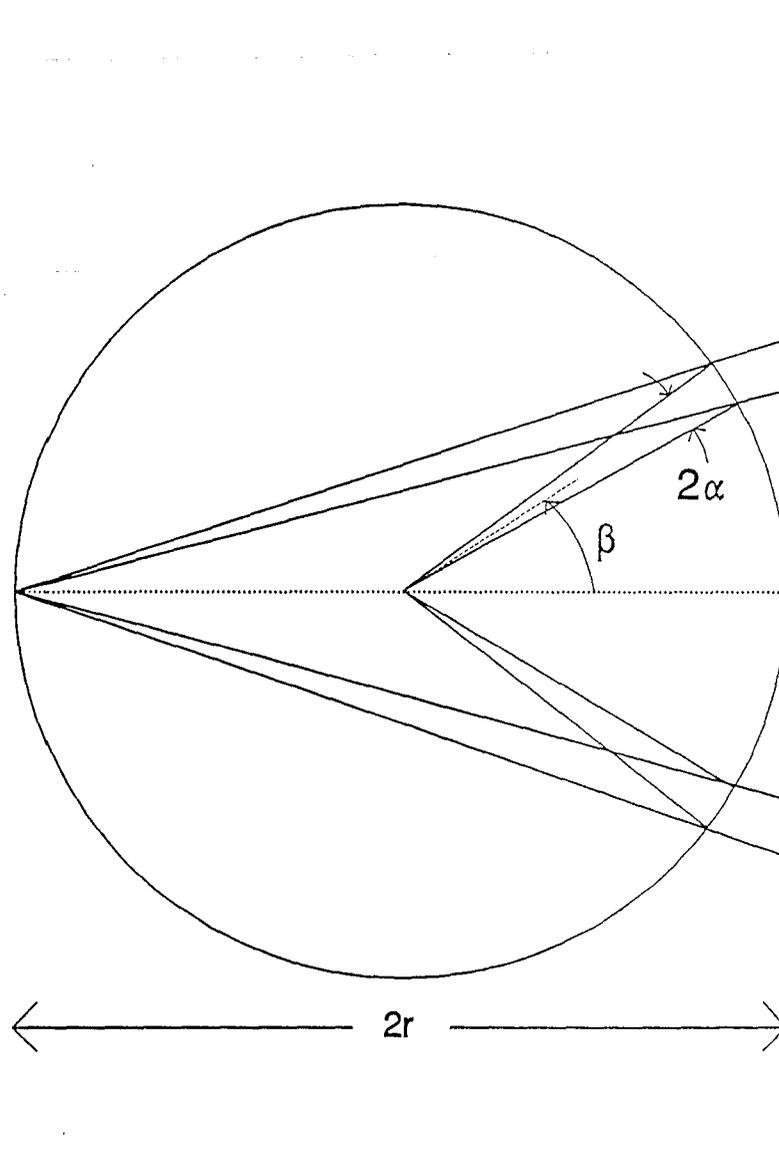
Figure 5. The stereographic projection in 2 dimensions.

Having established a problem, let us now offer a solution. If we rotate the structure 180° about the y axis, then the angle that was formerly $\theta = \pi$, is now $\theta = 0$. By carrying out the same transformation on the rotated structure, we can simply eliminate the singularity. A diagram of this is shown in Figure 6. In looking at the diagram, it is obvious that the field in the backward direction is much smaller than that in the forward direction, since the conductors in the projected plane are much further apart. This is the expected result. Since the ordinary transformation is called a stereographic transformation, let us call the procedure where we include the 180° rotation to be a reverse stereographic transformation.

The net effect of the reverse stereographic transformation is to replace θ with $\pi - \theta$. Thus, after one has found the projection for the forward direction, it is straightforward to replace θ with $\pi - \theta$ to get the reverse transformation. This point will be referred to several times later in this paper.
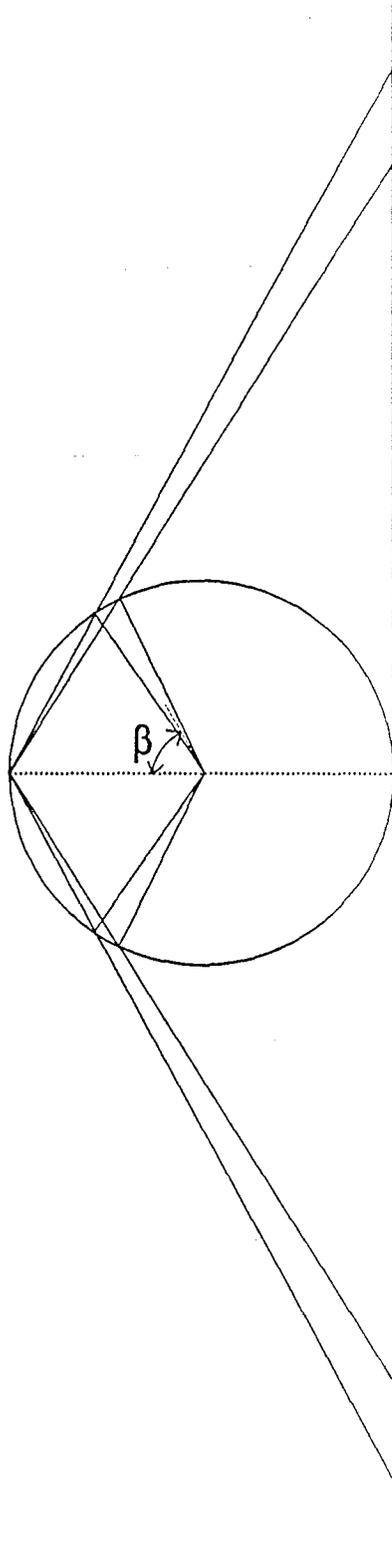
Figure 6. The reverse stereographic projection.

III. First Case: Bent Circular Cones

We now apply the forward and reverse stereographic transformations to the case of bent circular cones. Consider again the geometry of Figure 3. The intersection of the two circular cones with a sphere of radius r_o is two circles. These are then projected onto the plane using (3). It is shown in [7] that the projection is again two circles, arranged as in Figure 7, with radii a and distance between centers $2b$, where

$$b = \frac{2 r_o \sin(\beta)}{\cos(\alpha) + \cos(\beta)}$$

$$a = \frac{2 r_o \sin(\alpha)}{\cos(\alpha) + \cos(\beta)}$$

(5)

The propagation characteristics of this geometry are well known. The characteristic impedance is $Z_c = f_g Z_o$, where $Z_o \simeq 377 \; \Omega$ and

$$f_g = \frac{1}{\pi} \operatorname{arccosh}(b/a)$$

(6)

Since $b/a = \sin(\beta)/\sin(\alpha)$, the above simplifies to

$$f_g = \frac{1}{\pi} \operatorname{arccosh}\left[\frac{\sin(\beta)}{\sin(\alpha)}\right]$$

(7)

Furthermore, the electric field in the center of the projected plane, at $(x,y) = (0,0)$ has been derived previously in [11]. Thus,

$$E_y = -\frac{2V}{b} \frac{1}{\operatorname{arccosh}(b/a)} \frac{1}{\sqrt{1-(a/b)^2}}$$

(8)

This field assumes a voltage $+V$ on the top conductor and $-V$ on the bottom conductor. The above is now combined with (5) and (6) to get

$$E_y = -\frac{V}{r_o} \frac{\cos(\alpha) + \cos(\beta)}{\pi f_g \; \tanh(\pi f_g) \; \sin(\beta)}$$

(9)

This is exactly the field in the center of the bent circular cones at $\theta = 0$. Thus, in spherical coordinates we have

$$E_\theta(\theta=0, \phi=\pi/2) = -\frac{V}{r_o} \frac{\cos(\alpha) + \cos(\beta)}{\pi f_g \; \tanh(\pi f_g) \; \sin(\beta)}$$

(10)

Note that the return to spherical coordinates is trivial since we are at the polar axis. If we were away from $\theta = 0$ an adjustment would have to be made.

2 a

b_o b
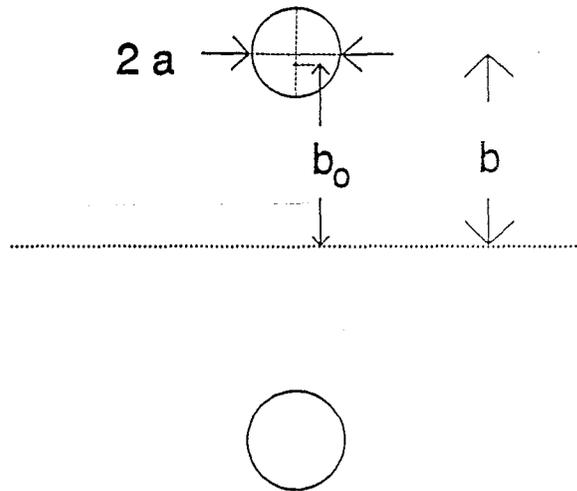
Figure 7. Projection of two bent circular cones onto a plane.

$D^2/(16F)$

β_o

$\leftarrow$ F $\longrightarrow$
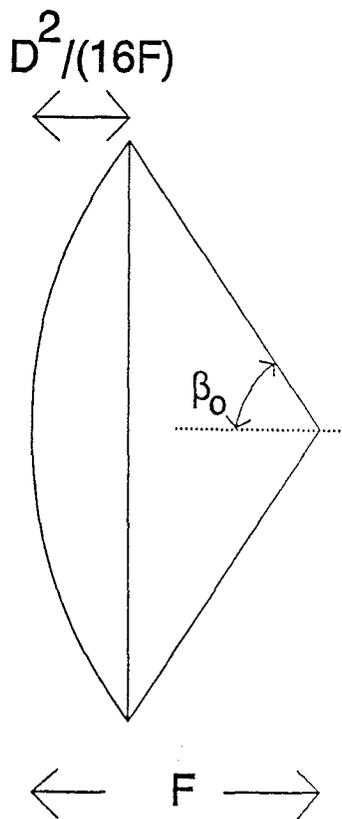
Figure 8. Side view of an IRA.

In order to find the field at $\theta = \pi$, we now need to invoke the reverse stereographic projection. As was demonstrated in the previous section, it is now only necessary to replace β with $\pi-\beta$ in the above equation. Thus we find

$$E_\theta(\theta=\pi,\phi=\pi/2) = -\frac{V}{r_o}\frac{\cos(\alpha)-\cos(\beta)}{\pi f_g \tanh(\pi f_g) \sin(\beta)} \tag{11}$$

The front/back ratio, η, for this feed may be found simply as

$$\eta = \frac{E_\theta(\theta=0)}{E_\theta(\theta=\pi)} = \frac{\cos(\alpha)+\cos(\beta)}{\cos(\alpha)-\cos(\beta)} = \cot((\beta+\alpha)/2)\cot((\beta-\alpha)/2) \tag{12}$$

This fully characterizes the bent circular cone feed.

The next step in the analysis is to specify the correct alignment of the feed with the edge of the parabolic reflector. It was shown in [4] that the feed needs to meet the edge of the reflector at the same point as a thin line charge would. A diagram of this is shown in Figure 8. This height, b_o, is shown in [4] to be $(b^2-a^2)^{1/2}$, or using (6),

$$b_o = b \tanh(\pi f_g) \tag{13}$$

If we refer now to Figure 8, we find from simple geometry the angle from the center axis to the edge of the dish, is

$$\beta_o = \arctan\left[\frac{1}{2f_d - 1/(8f_d)}\right] \tag{14}$$

where we have defined $f_d=F/D$, the ratio of focal length to diameter of the reflector. Next, we find β using (3) and (13) as

$$\beta = 2\arctan\left[\frac{\tan(\beta_o/2)}{\tanh(\pi f_g)}\right] \tag{15}$$

Having β, we now find α from (7) as

$$\alpha = \arcsin\left[\frac{\sin(\beta)}{\cosh(\pi f_g)}\right] \tag{16}$$

Thus, we have specified all angles for a given f_g and f_d.

It is helpful at this point to provide an example for a typical configuration. Consider once again the side view of an IRA as shown in Figure 8. Let us assume we are interested in a 400 Ω feed for a parabolic reflector with $f_d = F/D = 0.4$. Using (14-16), we find $\beta_o = 64.01^o$, $\beta = 64.14^o$, and $\alpha = 3.68^o$. Substituting these values into (10-12), we find

$$E_\theta(\theta=0, \phi=\pi/2) \quad = \quad -\frac{V}{r_o} \, 0.479 \tag{17}$$

for the forward direction and

$$E_\theta(\theta=\pi, \phi=\pi/2) \quad = \quad -\frac{V}{r_o} \, 0.188 \tag{18}$$

for the reverse direction, which says that the front/back ratio is $\eta = 2.55$.

IV. Second Case: Coplanar Conical Plates

A second case we would like to develop is that of two coplanar conical plates. This geometry, which is shown in Figure 9, has the advantage that it provides minimal optical blockage of the dish. After invoking the stereographic transformation (2,3), the two-dimensional cylindrical problem becomes that of Figure 10(a), where

$$b_1 = 2r_o \tan(\beta_1/2)$$

$$b_2 = 2r_o \tan(\beta_2/2)$$

(19)

We now introduce a clockwise rotation of 90°, as shown in Figure 10(b). This geometry conforms to one provided by Moon and Spencer [12], Figure 2.16. This figure is reproduced in approximate form in Figure 11. The conformal mapping is

$$w(z) = \text{sn}^{-1}(z/b_1)$$

(20)

where the function sn(z) is one of the Jacobian elliptic functions, as defined in [13], and the notation $\text{sn}^{-1}(z)$ indicates the inverse sn function. Implicit in the definition of the elliptic functions is a parameter k, which is

$$k = \frac{b_1}{b_2} = \frac{\tan(\beta_1/2)}{\tan(\beta_2/2)} \equiv m^{1/2}$$

(21)

for our configuration. Thus, the notations sn(z) and sn(z|m) are equivalent.

The characteristic impedance of the structure in Figure 10(b) is now calculated by

$$Z_c = Z_o \frac{\Delta u}{\Delta v}$$

(22)

where $u(z)$ and $v(z)$ are the real and imaginary parts of $w(z)$ in (20), and $Z_o \simeq 377\Omega$. Furthermore, Δu is the change in u from the first conductor to the second. From Figure 11, this is 2K(m), where K(m) is the complete elliptic integral of the first kind as defined in [13], 16.1.1 and 17.3.1. In addition, Δv is the change in v around one of the conductors, or 2K'(m), where K'(m)=K(1-m). Thus, the impedance of this structure is

$$Z_c = Z_o \frac{K(m)}{K'(m)}$$

(23)

or expressed as a geometric factor,

$$f_g = \frac{K(m)}{K'(m)}$$

(24)

If the feed impedance Z_c is known, then m can be found with this equation, since tables of m versus K'(m)/K(m) exist, for example in [13], Table 17.3.

$2\alpha'$

β_2

β_0

β_1

Side

Front
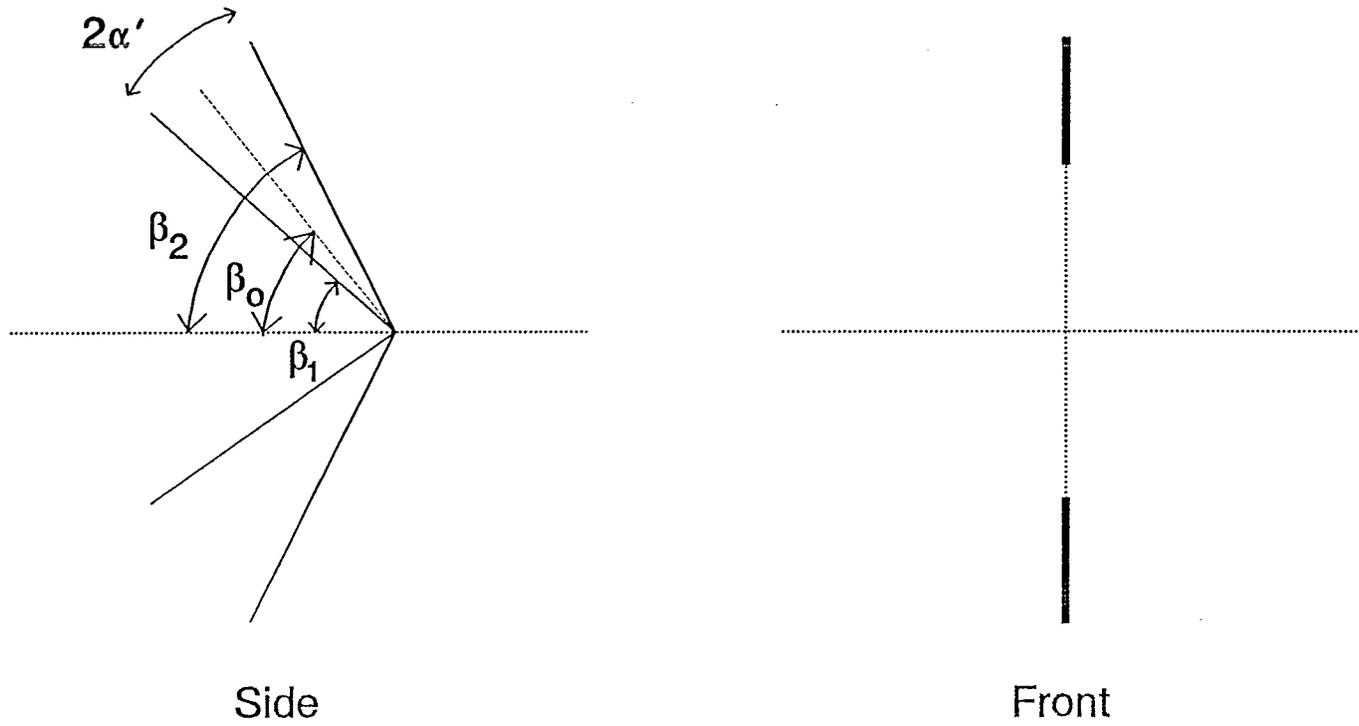
Figure 9. Coplanar conical plates.

b_2

b_o

b_1

(a)

(b)
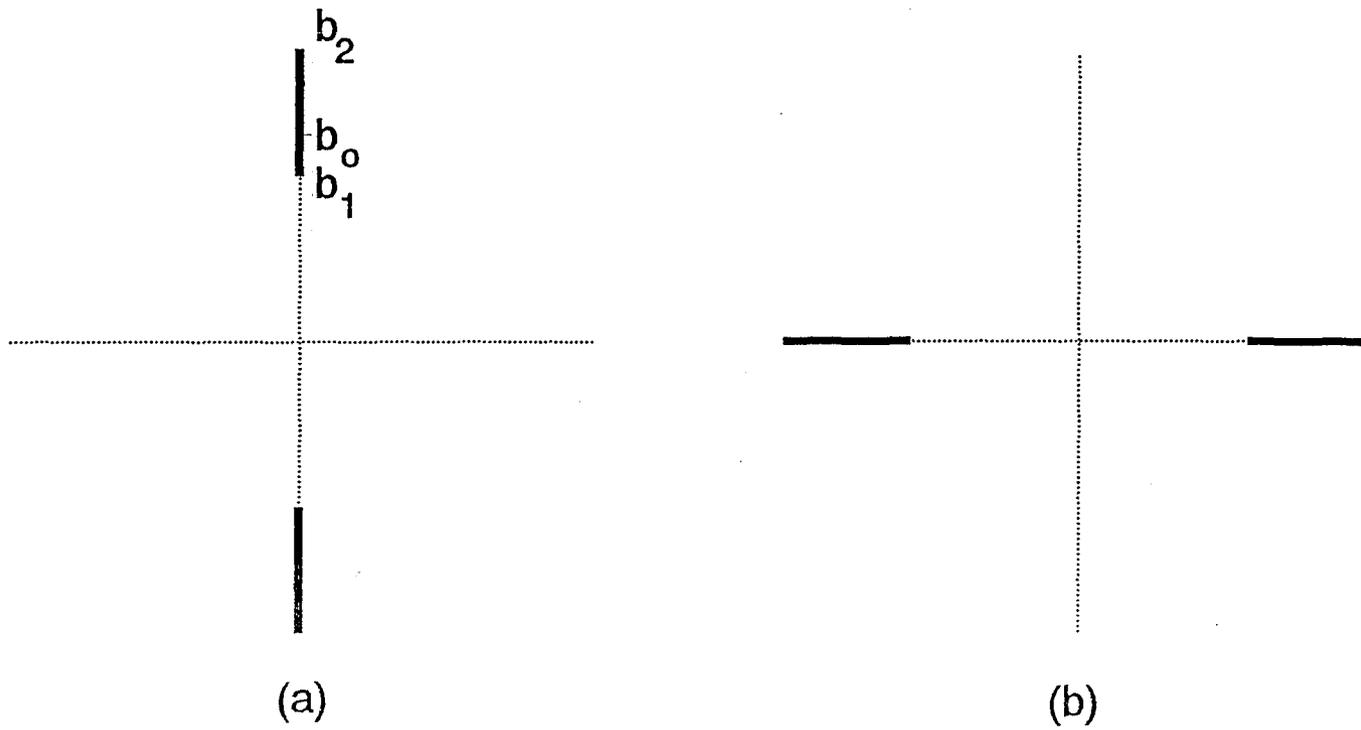
Figure 10. Projection of the coplanar conical plates before (a) and after (b) a 90° rotation.

Y

u=0

v=K'/2

v=0

v=K'   X

u=-K

u=K

b_1

b_2

$b_1 / b_2 = k$
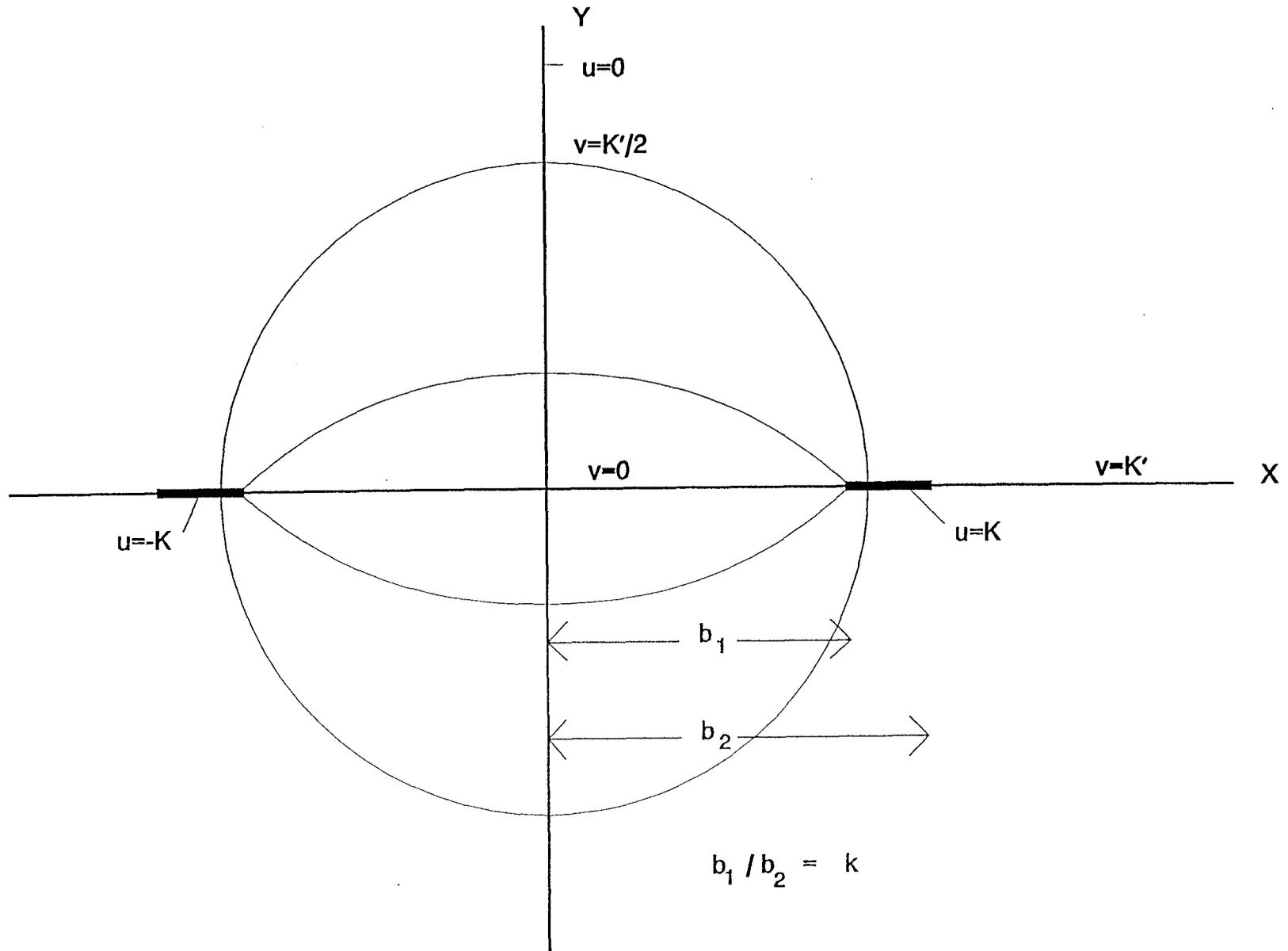
Figure 11.   An approximation of the sn curves, $w(z) = sn^{-1}(z/b_1)$. Note that a more detailed diagram is available in [12].

Next, we need to find the field at the center of the structure in the projected plane. From Figure 11, at $(x,y)=(0,0)$ the electric field parallel to the plates is

$$E_x(0,0) = - \frac{V}{K(m)} \frac{\partial u(z)}{\partial x} \Big|_{z=0} \tag{25}$$

where again the plates are charged with $+V$ and $-V$ on the right and left, respectively. We can now use the conformal mapping (20) and the fact that $v(z)=0$ and $y=0$ at the center, to find

$$u(x) = \text{sn}^{-1}(x/b_1) \tag{26}$$

The derivative is calculated using an expression from reference [13] equation 17.4.45,

$$\text{sn}^{-1}(x/b \mid b^2/a^2) = a \int_0^x \frac{dt}{[(a^2 - t^2)(b^2 - t^2)]^{1/2}} \tag{27}$$

After taking the derivative of the above equation, and evaluating it for $z=0$, we find

$$\frac{\partial u(x)}{\partial x} = \frac{1}{b_1} \tag{28}$$

Hence, $E_x(0,0) = -V / [b_1 K(m)]$, or substituting in for b_1 and returning to spherical coordinates,

$$E_\theta(\theta=0, \phi=\pi/2) = - \frac{V}{r_o} \frac{1}{2 K(m) \tan(\beta_1/2)} \tag{29}$$

where

$$m = \frac{\tan^2(\beta_1/2)}{\tan^2(\beta_2/2)} \tag{30}$$

Note again that the return to spherical coordinates is trivial since we are at the polar axis.

To find the field in the reverse direction, we once again invoke the reverse stereographic projection, as described in Section II. In order to keep the notation orderly, we add an additional subscript r to all angles and projections of angles that are used in the reverse stereographic projection. Thus, one may adapt the forward stereographic projection into the reverse one as

$$\beta_{1r} = \pi - \beta_2$$

$$\beta_{2r} = \pi - \beta_1 \tag{31}$$

for the angles, and

20

$$b_{1r} = 2r_o \tan((\pi - \beta_2)/2) = 2r_o \cot(\beta_2/2)$$

$$b_{2r} = 2r_o \tan((\pi - \beta_1)/2) = 2r_o \cot(\beta_1/2)$$

(32)

for the projections. Now it is simple to find the field for the reverse direction by replacing angles and projections for the forward case with those for the reverse case, subscripted by r. Thus we find for the field in the reverse direction

$$E_\theta(\theta = \pi, \phi = \pi/2) = -\frac{V}{r_o} \frac{1}{2K(m) \tan(\beta_{1r}/2)}$$

$$= -\frac{V}{r_o} \frac{1}{2K(m) \cot(\beta_2/2)}$$

(33)

The equation for m remains the same for the reverse direction as it is for the forward direction. Thus a front/back ratio for the feed may be simply expressed as

$$\eta = \cot(\beta_1/2) \cot(\beta_2/2)$$

(34)

Note the similarity between this front/back ratio, and that given previously for the bent circular cones in (12).

It is now necessary to identify the point on the feed that will be in contact with the edge of the dish. As we have seen previously, this is not necessarily at the center of the plate, but at a slightly lower position, $y = b_o$. The angle from the plane of symmetry to b_o is specified as β_o. We once again calculate this angle from simple geometry, using the focal length and reflector diameter, to find

$$\beta_o = \arctan\left[\frac{1}{2f_d - 1/(8f_d)}\right]$$

(35)

Next, we need to find the correct position on the projection plane to correlate with this angle. From Figure 11, which shows the transform in the projection plane, we see that if $v(z) = \frac{1}{2}K'$ the contour is circular, thus matching the edge of a circular reflector. This occurs at

$$b_o = \sqrt{b_1 b_2} = b_1/\sqrt{k}$$

(36)

where b_o is the projection of β_o. Using the stereographic transform (3), this becomes

$$\tan(\beta_o/2) = (1/\sqrt{k}) \tan(\beta_1/2)$$

(37)

or

$$\beta_1 = 2 \arctan(\sqrt{k} \tan(\beta_o/2)) \tag{38}$$

Finally, since $b_2/b_1 = 1/k$, and using once again the stereographic projection (3),

$$\beta_2 = 2 \arctan(\tan(\beta_1/2)/k) \tag{39}$$

Thus, we have completely specified all the relevant angles of the geometry for a given f_g and f_d.

It is helpful at this point to once again provide an example. Again, let us consider the case where $Z_c = 400\ \Omega$, F/D=0.4, and D=1. Since $f_g = 1.061$ is known, we can find m from (24) and Table 17.3 of [13], which gives K'(m)/K(m) as a function of m. Interpolating from the table, we find $m = 0.5645$, and therefore $k = m^{1/2} = 0.7513$. The angle β_o is calculated from (35), so $\beta_o = 64.01°$. The angles β_1 and β_2 are found from (38-39) to be 56.89° and 71.59°, respectively. The fields in the forward and reverse directions are provided in (29) and (33). From Reference [13] Table 17.1 we find the complete elliptic integral K($m = .5645$) = 1.913, so

$$E_\theta(\theta=0, \phi=\pi/2) = -\frac{V}{r_o} 0.4825 \tag{40}$$

$$E_\theta(\theta=\pi, \phi=\pi/2) = -\frac{V}{r_o} 0.1885 \tag{41}$$

This gives a front/back ratio of $\eta = 2.56$. Note that these results are very similar to those for the bent circular cones of the previous section. This is to be expected for two feeds of the same impedance. Note also that $\beta_2 - \beta_1 = 14.7°$, which is about twice the value of $2\alpha = 7.36°$ in the previous problem. This is also to be expected, since it is well known that a thin strip behaves asymptotically like a rod whose diameter is half the strip width. This point is proven in Appendix B of this paper.

V. Comparison of Prepulse Area to Impulse Area

Now that we can calculate easily the prepulse fields for two configurations, let us compare the area of the prepulse to the area of the impulse. If they are equal, then that will allow us to say certain things about the tail in the part of the waveform that follows the impulse. Recall once again the diagram of an ideal signal shown in Figure 2.

We use here the model for the bent circular cone, although as we have just seen, results for the coplanar conical plates would be similar. Again, let us use a feed impedance of 400 Ω, and assume that the parabolic reflector is round. The area under the prepulse is found by integrating (11) to find

$$A_p = \int_0^{2F/c} E_\theta \, dt$$

$$= - \frac{V}{r_o} \frac{2F}{c} \frac{\cos(\alpha) - \cos(\beta)}{\pi f_g \, \tanh(\pi f_g) \, \sin(\beta)} \tag{42}$$

The field on axis due to the impulse is found in [4] as

$$\vec{E} = \frac{V}{r_o} \frac{\delta_a(t)}{\pi c f_g} \vec{h}_a \tag{43}$$

where $\vec{h}_a$ is an effective height and $\delta_a(t)$ is an approximate form of the Dirac delta function. Note that V in this paper is the voltage from the plane of symmetry to one of the conductors, whereas in [4] V is the total voltage between conductors. Note also that there are some theoretical problems in the near field with a radiating field proportional to $\delta(t)$ in the far field. Thus, we use here $\delta_a(t)$ to describe the time dependence, where $\delta_a(t)$ is a function whose integral is 1 but whose maximum amplitude is finite and dependent upon r. This problem is explained in more detail in [1] and [4].

Since our reflector is round, the effective height is calculated in [4] to be $\vec{h}_a = D/2 \, \vec{1}_\theta$. After making this substitution and performing the integration with respect to time, we find for the impulse area is

$$A_i = \frac{V}{r_o} \frac{D}{2\pi c f_g} \tag{44}$$

Not that this calculation was originally done in [4] for the limit of a long feed. In Appendix A of this paper this result is extended to feeds of arbitrary length. The ratio of the prepulse area to the impulse area is now easily found as

23

$$\left| \frac{A_p}{A_i} \right| \ = \ \frac{4 f_d \, [\, \cos(\alpha) - \cos(\beta) \,]}{\tanh(\pi f_g) \ \sin(\beta)} \tag{45}$$

Continuing with our previous example, with $f_d = 0.4$, and $Z_c = 400 \ \Omega$, we find this ratio is equal to 1 to four decimal places. Hence for our typical example, we are for all practical purposes at a point where the areas are equal.

We now examine the dependence of the area ratio upon the feed impedance and the f_d. In Figure 12 we have plotted $|A_p/A_i| - 1$ versus f_d for three different feed impedances. For the cases of either 200Ω or 400Ω feeds, almost any feed length provides an area ratio near unity.
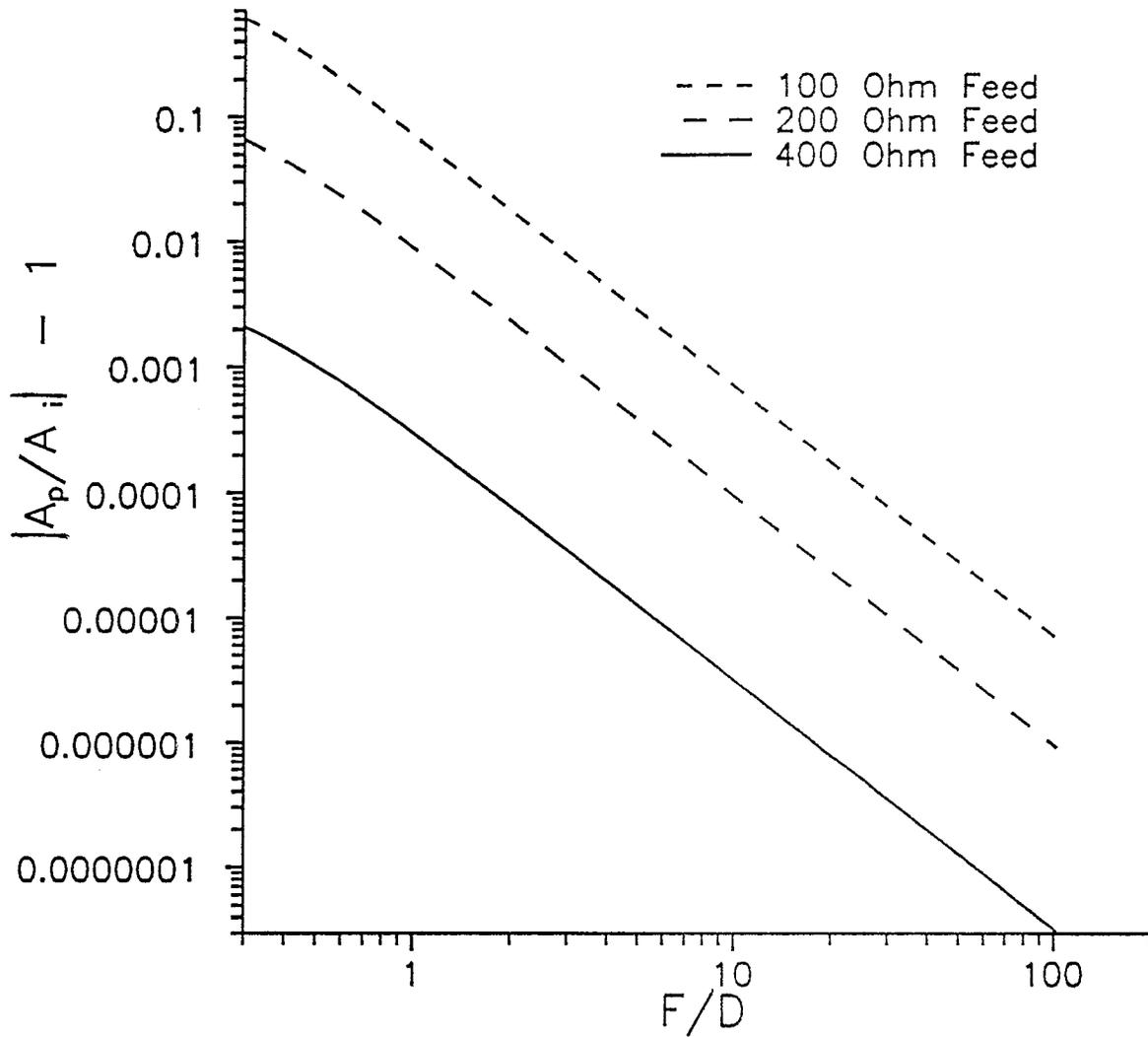
Figure 12. Variation of $|A_i/A_p|$, the ratio of the impulse area to the prepulse area, with F/D for three feed impedances.

VI. Analysis

Our results indicate that for a typical case, the areas under the prepulse and impulse are approximately equal. This suggests that if the prepulse and impulse areas are equal, or nearly so, then the total area under the tail portion of the curve is also nearly equal to zero. This must be true because the area under the overall waveform must be zero. What this means in practice is that if the feed terminations on an IRA are tuned properly, it should be possible to reduce the tail to something small.

We should point out, however, that the area calculations for both the prepulse and the impulse have certain approximations built into them. The approximations in the prepulse calculation include an assumption that there is no additional structure near the feed point, something that probably will not be true in a real system that may require voltage standoff protection for transmit mode. The approximation for the impulse calculation neglects the contribution from the interaction of the wavefront from the reflector with the feed structure. However, for large distances r to the observer on boresight (for which the impulse width $\rightarrow 0$ [1,4]), it is only for times such that these contributions can arrive at essentially the same time as the wavefront that they should be included here (instead of in the tail). In an asymptotic sense then a high-frequency approximation (i.e. geometrical theory of diffraction) is appropriate. This leads to a correction to $\overrightarrow{h}_a$ by removal of the integral of the portion of the TEM wavefront which intercepts the feed structure. This can be defined as the optical blockage of the feed. Of course, one may reduce the optical blockage of the feed by using the coplanar conical plate feed, but there will still be some coupling back onto the feed. As time goes on, the tail will, of course, be influenced by the currents induced on the feed structure, as well as the change in the currents (away from the simple, i.e. optical, currents) on the reflector.

VII. Conclusions and Recommendations

Simple analytic forms have been generated for the prepulse associated with the TEM feed of an IRA. These have been generated for two feed geometries, two circular bent cones, and two coplanar conical plates. For the two geometries we found similar fields and front/back ratios for the same feed impedance.

The prepulse fields were compared to the main impulse field by comparing their areas. The area under the prepulse was about the same as the area under the impulse, for either a 200Ω or 400Ω feed. Since the total area under the curve for the radiated field must be zero, this suggests that the tail expected to occur after the impulse will probably have a small amplitude if the matching circuit is tuned properly. An important next step in the development of the IRA will therefore be to lay out the design principles for the matching network at the junction of the TEM feed and the reflector.

It may seem fortuitous that the circular aperture area leads to the approximate cancellation of the prepulse and impulse areas. However, in [4] it was shown that the result of $\vec{h}_a = \vec{h}_{eq}/2$ applies not only to the circular aperture (with feed meeting the edge), but to an infinite aperture as well. This implies reflection of all the fields reaching an infinite paraboloidal reflector. Fortunately, a circular paraboloidal reflector, as a body of revolution, also permits two orthogonal planes of symmetry (containing the axis) for use with the dual-polarization (and impedance-transforming) feed discussed in [3].

Appendix A. Validity of the Impulse Area Calculation

In this paper we have compared the area of the prepulse to the area of the impulse for a typical IRA. The area under the impulse was calculated using some results from [4], however those results were derived only for long F/D's. The purpose of this appendix is to demonstrate that the results in [4] are general for any F/D. In doing so, we will prove that a paraboloidal reflector is a device that carries out the stereographic transform that is central to this paper. Hence, the reflector converts a spherical TEM wave to a planar TEM wave in a manner equivalent to the stereographic projection used in section II.

Let us consider now the first method of converting a spherical TEM wave to a plane wave, that of the stereographic projection. Assume that a conical transmission line has on it a potential $V(\theta,\phi)$. Now if we define a polar radius Ψ such that $\Psi = (x^2 + y^2)^{1/2}$, then according to the standard stereographic projection defined earlier in (3),

$$\Psi = 2F \tan(\theta/2) \tag{46}$$

The polar coordinate ϕ remains unchanged in this transformation. Therefore, the stereographic transformation may be carried out as

$$V(\Psi,\phi) = V(\theta,\phi) \Big|_{\theta = 2\arctan(\Psi/2F)} \tag{47}$$

The electric field in this aperture is just the gradient of the above potential in polar coordinates. Thus

$$\overline{E}^{(ap)}(\Psi,\phi) = -\nabla V$$

$$= \left[- \hat{1}_\Psi \frac{\partial V}{\partial \Psi} - \hat{1}_\phi \frac{1}{\Psi} \frac{\partial V}{\partial \phi} \right]_{\theta = 2\arctan(\Psi/(2F))} \tag{48}$$

This is the aperture field calculated by using the stereographic transform. Let us now consider the field generated by reflection off a paraboloid.

In order to calculate the reflected field, refer to Figure 13. Consider a ray emanating from the focus and reflecting off the paraboloidal surface. The field generated by the potential $V(\theta,\phi)$ at the reflector is

$$\overline{E}^{(inc)}(r_p,\theta,\phi) = -\frac{1}{r_p} \nabla_t V(\theta,\phi) \tag{49}$$

where r_p is the spherical radial distance from the focus to the paraboloid, and the transverse gradient is defined by

28
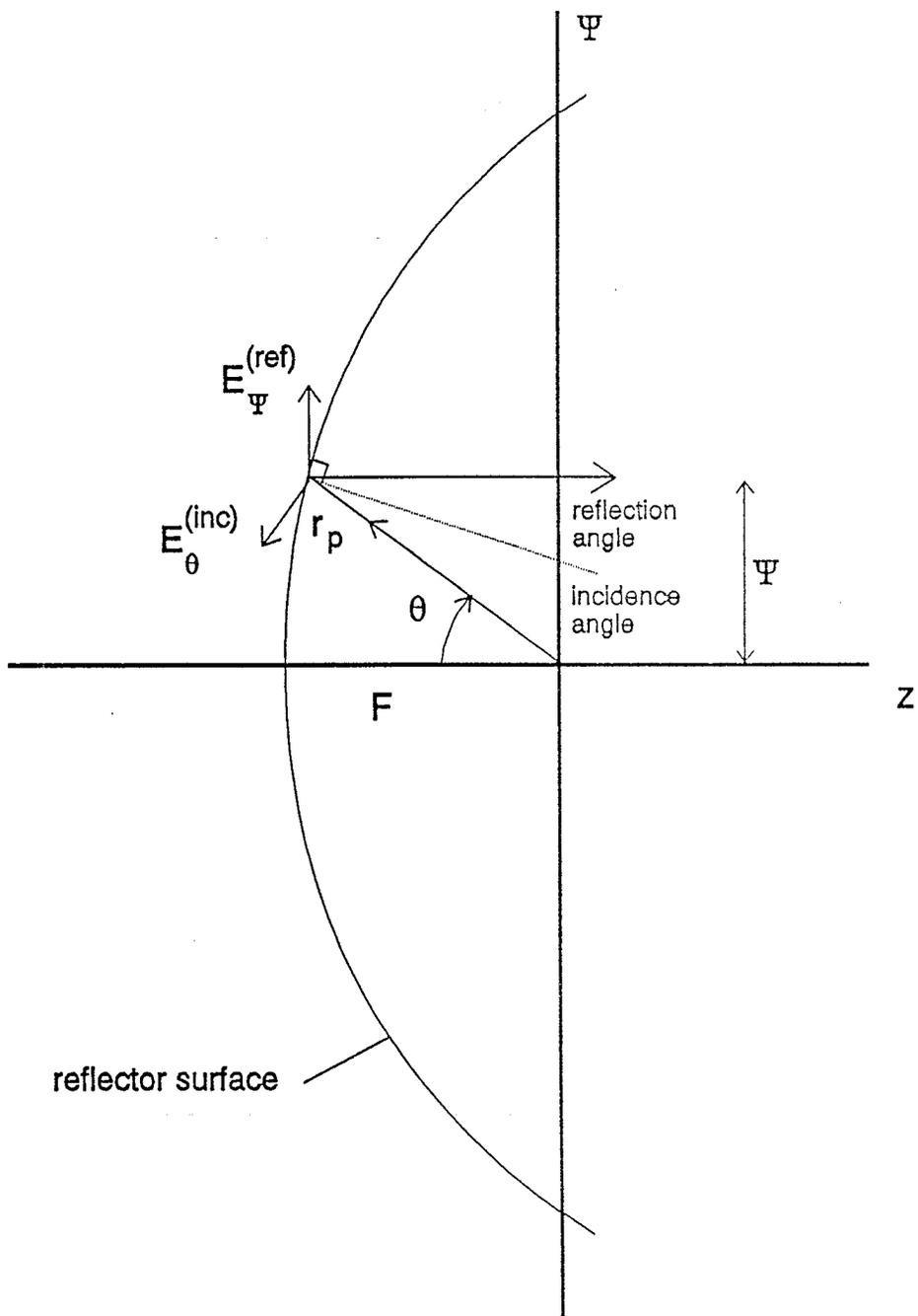
Figure 13. The incident and reflected rays for a paraboloidal reflector.

$$\nabla_t = \overline{1}_\theta \frac{\partial}{\partial \theta} + \frac{1}{\sin(\theta)} \overline{1}_\phi \frac{\partial}{\partial \phi} \tag{50}$$

These formulas are taken from [7]. A paraboloid is described by the formula [17]

$$r_p = \frac{2F}{1 + \cos(\theta)} \tag{51}$$

Furthermore, we have from simple geometry $\Psi = r_\text{p} \sin(\theta)$. Combining this with the above equation gives

$$\Psi = 2F \tan(\theta/2) \tag{52}$$

a result that by now may look familiar. Thus, the field incident upon the paraboloid is

$$\overline{E}^{(inc)} (\Psi,\phi) = -\frac{\sin(\theta)}{\Psi} \frac{\partial V}{\partial \theta} \overline{1}_\theta - \frac{1}{\Psi} \frac{\partial V}{\partial \phi} \overline{1}_\phi \tag{53}$$

It now remains only for us to calculate the field reflected from the paraboloid.

In order to calculate the reflected field, we note that the angle of reflection is equal to the angle of incidence, and that there is a reversal in sign at the conductor. Thus, we have

$$E_\phi^{(ref)} = -E_\phi^{(inc)}$$
$$E_\Psi^{(ref)} = -E_\theta^{(inc)} \tag{54}$$

This leads to a field reflected off the paraboloid as

$$\overline{E}^{(ref)} (\Psi,\phi) = -\frac{\sin(\theta)}{\Psi} \frac{\partial V}{\partial \theta} \overline{1}_\Psi + \frac{1}{\Psi} \frac{\partial V}{\partial \phi} \overline{1}_\phi \tag{55}$$

Furthermore, it simple to show using (52) that

$$\frac{\partial V}{\partial \theta} = \frac{\partial V}{\partial \Psi} \frac{\partial \Psi}{\partial \theta}$$
$$= \frac{\partial V}{\partial \Psi} \frac{\Psi}{\sin(\theta)} \tag{56}$$

so the final expression for the reflected field calculated as a reflection from the paraboloid is

$$\overline{E}^{(ref)} (\Psi,\phi) = \left[\frac{\partial V(\theta,\phi)}{\partial \Psi} \overline{1}_\Psi + \frac{1}{\Psi} \frac{\partial V(\theta,\phi)}{\partial \phi} \overline{1}_\phi \right]_{\theta = 2 \arctan(\Psi/(2F))} \tag{57}$$

$$= \nabla_{\Psi,\phi} V \Big|_{z = \text{constant}}$$

This is the same result obtained by stereographic projection in (48), to within a minus sign.

It is necessary now to propagate the ray from the surface of the paraboloid to some aperture plane perpendicular to the z-axis. We note that this reflected ray propagates parallel to the z-axis, and has a divergence factor of unity. This last point means that the field in the ray is neither increasing or decreasing in magnitude. These results are basic results of geometric optics, and can be derived using the techniques of any text on the subject, such as [19]. Furthermore, the total length (incident + reflected) of all rays starting at the focus and ending at some aperture plane is a constant, so there is no phase variation or time delay across the aperture. This leads to the conclusion that equation (57) describes not just the field on the paraboloid, but the aperture field as well.

Thus, the paraboloidal reflector is a physical device for carrying out the stereographic transform. The significance of this is as follows. The results derived in [4] for the impulse portion of the waveform were derived for a plane-wave over an aperture. In a practical case, however, it is likely that one will have a spherical TEM feed with a reflector. We have now shown the field on a spherical TEM feed to be equivalent to the planar aperture field used in [4]. Thus, the results generated in [4] for the planar TEM field are valid for our case of a spherical TEM feed and a paraboloidal reflector.

Since a paraboloidal reflector is now shown to be a physical device for implementing the stereographic transform of Section II, we might call this transform the Reflector Transform. In the present context note that this result applies for early times (or high frequencies) due to limitations associated with the feed and finite reflector size. Note that the stereographic transformation gives an equivalent way to calculate the potential function for a spherical TEM wave. It does not actually transform a physical spherical wave into a plane wave. In particular the phase of the wave (spherical wavefront) has to be changed into a plane wave. This can be done via a lens interposed between and connecting the conical transmission line and its equivalent (now actual) cylindrical transmission line. Examples of this are provided in reference [16] Appendix E.

Summarizing, we can now say

$$\text{lens transform} \equiv \text{stereographic transform (including lens)}$$
$$= -\text{reflector transform} \tag{58}$$

This gives us two general synthesis procedures for generating TEM plane waves from TEM spherical waves. Note that these transformations work in both directions by reciprocity, i.e. TEM plane waves can be transformed into TEM spherical waves (incoming).

Appendix B. Asymptotic Forms

At the end of Section IV of this paper, it was pointed out that for feed arms that are narrow in width, there is a simple relationship between the angular widths of the bent circular conical arms and the coplanar conical plate arms. In particular, it was noted that if the angular width of a plate were twice that of a circular cone, then the two structures would have the same feed impedance. We would now like to prove that assertion.

Let us first consider the asymptotic form of the bent circular cones. The geometric factor, f_g, as provided earlier, is

$$f_g = \frac{1}{\pi} \operatorname{arccosh}\left[\frac{\sin(\beta)}{\sin(\alpha)} \right] \tag{59}$$

As $\alpha \to 0$, $\sin(\alpha) \to \alpha$, so

$$f_g \to \frac{1}{\pi} \operatorname{arccosh}(\sin(\beta)/\alpha) \tag{60}$$

This can be simplified further as

$$f_g \to \frac{1}{\pi} \ln\left[\frac{2\sin(\beta)}{\alpha} \right] \tag{61}$$

This is a simple asymptotic form for the geometric factor of a bent circular cone feed.

Next, let us consider the asymptotic form for the conical coplanar plates. As was shown earlier, the geometric factor is

$$f_g = \frac{K(m)}{K'(m)} \tag{62}$$

where m is defined as

$$m = \left[\frac{\tan(\beta_1/2)}{\tan(\beta_2/2)} \right]^2 \tag{63}$$

and the angles are as shown in Figure 9.

Let us now recast the above equation in terms of a center angle and a half-angle width of the plates. Thus,

$$\begin{aligned}\beta_1 &= \beta - \alpha' \\ \beta_2 &= \beta + \alpha'\end{aligned} \qquad (64)$$

where α' is the half-angle width of the plate, and β is the angle to the center of the plate. If we expand (63) using these new angles, we find

$$\frac{\tan(\beta/2-\alpha'/2)}{\tan(\beta/2+\alpha'/2)} = \frac{\tan(\beta/2) - \tan(\alpha'/2)}{\tan(\beta/2) + \tan(\alpha'/2)} \frac{1 - \tan(\beta/2)\tan(\alpha'/2)}{1 + \tan(\beta/2)\tan(\alpha'/2)} \qquad (65)$$

If $\alpha \to 0$, this simplifies to

$$\begin{aligned}\frac{\tan(\beta/2-\alpha'/2)}{\tan(\beta/2+\alpha'/2)} &\to \frac{1 - (\alpha'/2)\cot(\beta/2)}{1 + (\alpha'/2)\cot(\beta/2)} \frac{1 - (\alpha'/2)\tan(\beta/2)}{1 + (\alpha'/2)\tan(\beta/2)} \\ &\to [\,1 - \alpha'\cot(\beta/2)\,][\,1 + \alpha'\tan(\beta/2)\,] \\ &\to 1 - \alpha'[\,\tan(\beta/2) + \cot(\beta/2)\,]\end{aligned} \qquad (66)$$

Furthermore, it is simple to show using [18] equation 403.02 that

$$\tan(\beta/2) + \cot(\beta/2) = \frac{2}{\sin(\beta)} \qquad (67)$$

so we have

$$m \equiv \frac{\tan^2(\beta/2-\alpha'/2)}{\tan^2(\beta/2+\alpha'/2)} \to 1 - \frac{4\alpha'}{\sin(\beta)} \qquad (68)$$

It now remains for us to simplify the elliptic integrals in (62).

In order to simplify the elliptic integrals we refer to [13], equation 17.3.21. Using this, we find

$$e^{-\pi K'/K} \to \frac{m}{16} \qquad (69)$$

as $m \to 0$. We now replace m with $1-m$ to find

$$e^{-\pi K/K'} \to \frac{1-m}{16} \qquad (70)$$

as $m \to 1$. This simplifies now to

$$\frac{K}{K'} \to \frac{1}{\pi}\ln\left[\frac{16}{1-m}\right] \qquad (71)$$

as $m \to 1$. Note that a similar expression may be found in Reference [14]. Since this is just our f_g, we may substitute the expression for m (68) to find

$$f_g \to \frac{1}{\pi} \ln \left[\frac{4 \sin(\beta)}{\alpha'} \right] \tag{72}$$

In comparing this result with (61), one gets the same geometric factor or impedance when $\alpha'=2\alpha$. This proves that if a coplanar conical plate feed has an angular width of twice that of a bent circular cone feed, then both feeds have the same impedance. This is true, of course, only in the limit of small α and if the center angle β's are the same.

References

1. C.E. Baum, Radiation of Impulse-Like Transient Fields, Sensor and Simulation Note 321, November 25, 1989.

2. E.G. Farr and J.S. Hofstra, An Incident Field Sensor for EMP Measurements, Sensor and Simulation Note 319, November 1989, and *IEEE Trans. Electromag. Compat.*, May 1991, vol. 33-2, pp. 105-112.

3. C.E. Baum, Configurations of TEM Feed for an IRA, Sensor and Simulation Note 327, April 27, 1991.

4. C.E. Baum, Aperture Efficiencies for IRAs, Sensor and Simulation Note 328, June 24, 1991, and 1992 URSI Symposium, Boulder, Colorado.

5. E.G. Farr, Analysis of an Impulse Radiating Antenna, Sensor and Simulation Note 329, July 1991.

6. W.S. Smythe, *Static and Dynamic Electricity*, Third Ed., Hemisphere, 1989, Sections 6.14 and 12.06.

7. R.W. Latham, M.I. Sancer, and A.D. Varvatsis, Matching a Particular Pulser to a Parallel-Plate Simulator, Circuit and Electromagnetic System Design Note 18, November 1974.

8. F.C. Yang and K.S.H. Lee, Impedance of a Two Conical-Plate Transmission Line, Sensor and Simulation Note 221, November 1976.

9. F.C. Yang and L. Marin, Field Distributions on a Two-Conical Plate and a Curved Cylindrical-Plate Transmission Line, Sensor and Simulation Note 229, September 1977.

10. D.V. Giri and C.E. Baum, Optimal Positioning of a Set of Peaker Arms in a Ground Plane, Circuit and Electromagnetic System Design Note 35, February 12, 1988.

11. C.E. Baum, Impedances and Field Distributions for Symmetrical Two Wire and Four Wire Transmission Line Simulators, Sensor and Simulation Note 27, October 10, 1966.

12. P. Moon and D.E. Spencer, *Field Theory Handbook*, 2nd Ed., Springer Verlag, p. 71, 1971.

13. M. Abramowitz and I.A. Stegun, *Handbook of Mathematical Functions*, National Bureau of Standards, AMS-55, Chapters 16 and 17, June 1964.

14.   C.E. Baum, A Conical-Transmission-Line Gap for a Cylindrical Loop, Sensor and Simulation Note 42, May 31, 1967.

15.   C.E. Baum, General Properties of Antennas, Sensor and Simulation Note 330, July 23, 1991.

16.   C.E. Baum and A.P. Stone, *Transient Lens Synthesis*, Hemisphere, 1990.

17.   G.B. Thomas, *Calculus and Analytic Geometry*, Addison-Wesley Publishing Co., Inc., 1972.

18.   H.B. Dwight, *Tables of Integrals and Other Mathematical Data*, Fourth Edition, Macmillan Publishing Co., Inc., 1961.

19.   P.H. Pathak, "Techniques for High Frequency Problems," Chapter 4 of *Antenna Handbook, Theory, Applications, and Design*, edited by Y.T. Lo and S.W. Lee, Van Nostrand Reinhold, 1988.